Kinetics of the ClO Self-Reaction and 210 nm Absorption Cross Section of the ClO Dimer

William J. Bloss, Scott L. Nickolaisen,† Ross J. Salawitch, Randall R. Friedl, and Stanley P. Sander*

Jet Propulsion Laboratory, California Institute of Technology, 4800 Oak Grove Drive, Pasadena, California 91109

Received: June 26, 2001; In Final Form: September 20, 2001

The kinetics of the dimerization of ClO radicals, ClO + ClO + M → Cl_2O_2 + M (1a), and the 210 nm absorption cross sections of the ClO dimer have been studied using the technique of flash photolysis with UV absorption spectroscopy, over the temperature range 183−245 K and pressure range 25−700 Torr. ClO radicals were generated following the photolysis of $Cl_2/Cl_2O/N_2$ mixtures and were quantified via their differential absorption between the peak of the (12,0) band of the ($\tilde{A} \leftarrow \tilde{X}$) transition at 275.2 nm and the adjacent minimum to higher wavelengths, while Cl_2O_2 formation was simultaneously monitored at 210 nm. ClO differential absorption cross sections were measured under identical conditions to the kinetic experiments by four separate calibration schemes. The rate coefficient measured at the lower temperatures studied (T < 200 K) was found to be up to 40% faster than extrapolation of previous results would suggest, with the limiting low- and high-pressure rate coefficients for reaction 1 in nitrogen determined to be $k_0 = (1.59 \pm 0.60) \times 10^{-32} \times (T/300)^{-4.50\pm0.98}$ molecules^{-2} cm^6 s^{-1} and $k_\infty = (1.36 \pm 0.22) \times 10^{-12} \times (T/300)^{-3.09\pm0.40}$ molecules^{-1} cm^3 s^{-1} respectively, obtained with $F_c = 0.6$. The corresponding value for k_0 in air is $k_{0(atm)} = (1.49 \pm 0.56) \times 10^{-32} \times (T/300)^{-4.50\pm0.98}$ molecules^{-2} cm^6 s^{-1}. The 210 nm absorption cross section of Cl_2O_2 was measured following time-resolved monitoring of its formation via ClO radical association, and a mean value of $(2.94 \pm 0.86) \times 10^{-18}$ molecule^{-1} cm^2 obtained, temperature independent (to within ± 15%) between 183 and 245 K. Errors are combined systematic uncertainties and 2 standard deviations statistical variation.

Introduction

The reactions of halogen oxide species are known to play a key role in determining the concentration and distribution of atmospheric ozone. The seasonal depletion of polar stratospheric ozone in the local spring (the formation of the "ozone hole") is attributed to gas-phase reactions of chlorine and bromine species whose concentrations are enhanced by heterogeneous processes. In particular, the catalytic ozone destruction cycle involving the ClO self-reaction is thought to be the dominant gas-phase ozone destruction process occurring in the Antarctic (and cold winter Arctic) stratosphere[1]

$$ClO + ClO + M \rightarrow Cl_2O_2 + M \quad (1a)$$

$$Cl_2O_2 + h\nu \rightarrow ClOO + Cl \quad (2)$$

$$ClOO + M \rightarrow Cl + O_2 + M \quad (3)$$

$$2 \times Cl + O_3 \rightarrow ClO + O_2 \quad (4)$$

$$\text{Net: } 2O_3 \rightarrow 3O_2$$

The rate of ozone loss through this catalytic cycle is determined by the rates of reactions 1a and 2, together with the ambient concentrations of Cl and O_3. The rate coefficient for reaction 1a and the absorption cross sections of Cl_2O_2 are thus of critical importance in attempts to quantify the depletion of polar stratospheric ozone using numerical models.

Kinetics of ClO + ClO. The ClO self-reaction is known to proceed through four channels,[2] a termolecular channel (1a), forming Cl_2O_2, and three bimolecular channels

$$ClO + ClO \rightarrow Cl_2 + O_2 \quad (1b)$$

$$\rightarrow Cl + ClOO \quad (1c)$$

$$\rightarrow Cl + OClO \quad (1d)$$

The ClO self-reaction was among the inaugural reactions to be studied using the flash photolysis technique,[3] and the occurrence of a recombination channel forming Cl_2O_2 was first postulated by Porter and Wright in 1953.[4] Subsequent studies elucidated the termolecular nature and room-temperature kinetics of reaction 1a.[5−7] The kinetics of the formation of Cl_2O_2 under the low-temperature and low-pressure conditions relevant to the polar stratosphere, investigated following recognition of the potential role of this chemistry in the atmosphere,[8] have been the subject of three studies: Hayman et al.,[9] Sander et al.,[10] Nickolaisen et al.,[11] and Trolier et al.[12] These studies are briefly described below. In all three cases (and in the current work), the kinetics of the ClO self-reaction was studied through photolytic reaction initiation (flash photolysis or molecular modulation spectroscopy) coupled with UV−vis absorption spectroscopy to quantify the radical species present. Thus, ClO absorption cross sections were required to determine absolute concentrations and hence obtain the second-order self-reaction rate coefficient.

* To whom correspondence should be addressed. E-mail: ssander@jpl.nasa.gov. Fax: 818 393 5019.

† California State University, 5151 State University Drive, Los Angeles, California 90032.

10.1021/jp012429y CCC: $20.00
Published on Web 11/28/2001

TABLE 1: Previous Determinations of k_{1a}: Conditions

study	year	technique	T/K (kinetics)	T/K (cross sections)	$[Cl_2]/10^{15}$ molecules^{-1} cm^3
Hayman et al.[9]	1986	molecular modulation	268−338	294−447[a]	36−360
Sander et al.[10]	1989	flash photolysis	195−247	220−400	2−5
Trolier et al.[12]	1990	flash photolysis	200−263	200−298	53−100
This Work	2001	flash photolysis	183−245	183−245	1−5

[a] Measured by Clyne and Coxon.[15]

TABLE 2: Previous Determinations of k_{1a}: Kinetics

study	k_0 (300 K)/10^{-32} molecules^{-2} cm^6 s^{-1}	n	k_∞ (300 K)/10^{-12} molecules^{-1} cm^3 s^{-1}	m	$k_{atm}/10^{-13}$ molecules^{-1} cm^3 s^{-1}
Hayman et al.[9]	$6.0^{+0.37}_{-0.34}$	2.1 ± 0.7	-		3.87
Sander et al.[10]	1.8 ± 0.5	3.6 ± 1.0	6.0 ± 2.0	0.0 ± 1.0	1.73
Trolier et al.[12a]	1.64 ± 0.09	4.4 ± 0.2	4.8 ± 0.5	0	2.06
Trolier et al.[12b]	1.34 ± 0.09	3.9 ± 0.3	8 ± 1.3	0	1.51
JPL 00−3[14]	2.2 ± 0.2	3.1 ± 0.2	3.4 ± 0.5	1.0 ± 1	1.69

k_{atm} is the calculated bimolecular rate coefficient for reaction 1a at 200K and 75 millibars/56 Torr (approximately equivalent to an altitude of 19km). All values except JPL 00−3 given for M ≡ N_2. Trolier et al. noted that incorporation of an intercept to their fall off curves gave a better fit to the experimental data. The first set of values given (a) for k_0, k_∞, and k_{atm} are those obtained excluding this intercept from their analysis, the second set (b) are those obtained when the intercept, given by $k_{int} = 2.7 \times 10^{-14} \times (T/300)^{-2.2}$ molecules^{-1} cm^3 s^{-1}, was included in the falloff fits.

The conditions and cross section measurements used in each of the previous studies are summarized in Table 1. The falloff behavior of association reactions such as the formation of Cl_2O_2 have been successfully described using the expressions developed from RRKM theory by Troe and co-workers,[13] and the kinetics of reaction 1a are commonly parametrized in terms of limiting low- and high-pressure rate coefficients, k_0 and k_∞, and a broadening factor F_c. The second-order rate coefficient for formation of Cl_2O_2, k_{1a}, is then given by

$$k_{1a}(T,[M]) = \frac{k_0[M]}{1+\left(\frac{k_0[M]}{k_\infty}\right)} \times F_c^{(1+[\log(k_0[M]/k_\infty)]^2)^{-1}} \qquad \text{(i)}$$

The value of 0.6 for F_c has been found to satisfactorily describe the falloff behavior of most atmospherically relevant reactions, while the temperature dependence of k_0 and k_∞ is given by

$$k_0(T) = k_0(300) \times (T/300)^{-n} \qquad \text{(ii)}$$

$$k_\infty(T) = k_\infty(300) \times (T/300)^{-m} \qquad \text{(iii)}$$

The values of k_0, k_∞, n, and m obtained in previous studies of reaction 1a are given in Table 2, together with the values from the JPL 00−3 evaluation, Sander et al.[14] Also listed are bimolecular rate coefficients (k_{atm}) calculated for reaction 1a using each of the parametrizations reported, for 200 K and 75 millibars of N_2, conditions approximately equivalent to the polar stratosphere at an altitude of 19 km.

Hayman et al.[9] investigated the kinetics of reaction 1 using a molecular modulation technique, monitoring ClO via absorption spectroscopy at 277.3 nm, the peak of the (11,0) band of the ($\tilde{A} \leftarrow \tilde{X}$) transition. They measured both pressure-dependent and pressure-independent components to the overall ClO decay, and reported values based upon analysis of data obtained at pressures below 25 Torr and at 4 temperatures from 268 to 338 K. Over this pressure range they observed a linear increase in k_{1a} with respect to pressure, thus their values can be equated to k_0, the low-pressure limit for k_{1a}, given in Table 2. Hayman et al. used an extrapolation of the expression for the temperature dependence of the ClO cross sections reported by Clyne and Coxon,[15] who measured a linear variation of σ(ClO) with temperature over the range 294−447 K. Subsequent studies[11,16] of the ClO cross sections measured on adjacent bandheads at comparable resolution have found curvature in the temperature dependence, with σ(ClO) increasing more rapidly below ambient temperature, indicating that the extrapolation used by Hayman et al. may not have been valid.

Sander et al.[10] employed broadband flash photolysis with UV absorption spectroscopy to study reaction 1. ClO radicals were generated by photolysis of Cl_2/Cl_2O mixtures in a variety of bath gases, and the decay of ClO radicals monitored via the absorption change at the peak of the (12,0) band at 275.2 nm. Sander et al. used ClO cross sections measured in the course of their earlier study of the ClO + BrO reaction,[16] over the temperature range 220−450 K, and extrapolated/interpolated these to conduct ClO + ClO kinetic measurements from 195 to 247 K.

Trolier et al.[12] also used the technique of flash photolysis/UV absorption, monitoring ClO principally through single-wavelength detection at the peak of the (9,0) band at 282.65 nm, together with a limited number of measurements performed using a diode array detection system to monitor the ClO spectrum between ca. 225 and 300 nm. Trolier et al. measured σ(ClO) by titrating (excess) ClO formed in a discharge with known concentrations of NO. Kinetic and cross section measurements were performed between 200 and 298 K. Trolier et al. found that the falloff curves obtained from fitting eq i to their kinetic data did not go through the origin ($k_{1a} > 0$ as [M] → 0), and performed a second analysis in which an arbitrary intercept was added to eq i to better describe their data. Results from both of these parametrizations are included in Table 2.

The studies described above all employed Cl_2 as a photolytic precursor to ClO radicals. Molecular chlorine is known to be an efficient third body for reaction 1a: Nickolaisen et al.[11] report an enhancement factor of 3.4 in k_{1a} for M = Cl_2 compared with M = N_2 at 300 K. Such an enhancement is greater than expected on the basis of a vibrational energy transfer mechanism, and has been attributed to occurrence of a chaperone mechanism[11]

$$ClO + Cl_2 \rightarrow ClO \bullet Cl_2 \qquad (5)$$

$$ClO + ClO \bullet Cl_2 \rightarrow Cl_2O_2 + Cl_2 \qquad (6)$$

As can be seen from Table 1, the $[Cl_2]$ present in the previous studies varies by up to 2 orders of magnitude. In particular, the study of Hayman et al.[9] is likely to have been affected by

high [Cl_2], thus these results may not be directly applicable to the atmosphere. Trolier et al. corrected their measured values of k_1 for the contribution from Cl_2-mediated reactions, measured to be $k_{1a} = 11 \times 10^{-32}$ mlecules^{-2} cm^6 s^{-1} at 200 K for M = Cl_2.

Considerable discrepancy exists between the existing studies of the rate of the ClO + ClO association reaction, with the "atmospheric" bimolecular rate coefficient k_{atm} varying from 1.74×10^{-13} (Sander[10]) to 2.19×10^{-13} (Trolier et al.[12]) or 3.87×10^{-13} (Hayman et al.,[9] extrapolated) molecules^{-1} cm^3 s^{-1} at 200 K (Table 2). The discrepancy in the values of k_0 is greatest at low temperatures, below ca. 210−220 K. Comparison between the values obtained for k_0 at the very lowest temperatures is complicated by the cross sections used: extrapolated below 294 K by Hayman et al.,[9] and below 220 K by Sander et al.,[10] and by the differing contributions made by Cl_2-mediated reactions.

Absorption Cross Sections of Cl_2O_2. The first measurement of the UV absorption spectrum of Cl_2O_2 was reported by Basco and Hunt[17] in 1979. Cross sections were reported by Molina and Molina[8] (subsequently shown[18] to be contaminated by Cl_2O_3), Cox and Hayman[19] and Permien et al.,[20] and more recently by DeMore and Tschuikow−Roux,[21] Burkholder et al.[18] and Huder and DeMore.[22] There is good agreement over the general shape of the cross section, and its value at the peak at 245 nm, although important discrepancies still exist concerning the magnitude of the "tail" region beyond 300 nm. All the previous cross section determinations have been performed using diode-array spectrometers or scanning spectrophotometers to record absorption spectra of mixtures of Cl_2O_2, ClO and precursor species (Cl_2 and either Cl_2O or O_3), the contributions from which were subsequently removed. Quantification of the loss of ClO radicals and/or the ClO precursor species enabled conversion of the resulting Cl_2O_2 absorption spectra to cross sections. ClO radicals (and hence Cl_2O_2) were generated by modulated photolysis over time scales of tens of seconds to minutes, or by discharge flow techniques over time scales of a few seconds. However, time-dependent formation of Cl_2O_2 from the association of ClO radicals under the conditions relevant to the stratosphere has not previously been observed, or used to directly determine Cl_2O_2 cross sections.

This study was motivated by the uncertainty in the reported values of k_{1a}, the need to measure the kinetics of reaction 1 at the very lowest temperatures found in the polar stratosphere, and in part to validate the extrapolation of ClO cross sections below 220 K adopted in the previous study from this laboratory. This work used the technique of flash photolysis to generate ClO radicals, and UV−vis absorption spectroscopy to monitor their decay and the concomitant formation of Cl_2O_2. The differential absorption of ClO radicals, between a band peak and the adjacent trough, was used to quantify ClO and, hence, obtain kinetic data. The absorption cross sections of Cl_2O_2 were then directly determined from the time-dependent evolution of the Cl_2O_2 absorption and ClO concentration.

The use of differential spectroscopy to quantify ClO radicals removes the need for correction of the measured absorption for the presence of other absorbing species (Cl_2O_2, Cl_2O, O_3) required in the previous (single wavelength) studies. Moreover, time-resolved monitoring of Cl_2O_2 formation eliminates many of the uncertainties inherent in the spectral stripping procedures employed in previous determinations of $\sigma(Cl_2O_2)$ and potential problems arising from wall losses of reactive species over the duration of the slower experiments.

Experimental Approach

The ClO self-reaction was studied using the technique of broadband flash photolysis with kinetic UV absorption spectroscopy. The apparatus has been described in detail previously[23,24] therefore only brief details are given here. A schematic diagram of the apparatus is shown in Figure 1.

The experimental system utilized a triple-jacketed Pyrex reaction cell, comprising reaction volume, temperature regulation envelope and flashlamp envelope arranged concentrically. The reaction cell was 120 cm in length, with an internal diameter (reaction volume) of 3 cm. Evacuated Pyrex endpieces fitted with antireflection coated windows were used to seal the reaction cell. The endpieces protruded approximately 15 cm into the reaction cell at each end, ensuring both a uniform photolysis flux throughout the reaction volume and thermal equilibration of the precursor gas mixture, which flowed along the narrow (0.5 mm) space between the endpiece and the cooling envelope wall. Temperature control was achieved through a circulating cooler, employing methanol (for reaction cell temperatures down to ca. 195 K) or the lower-viscosity pentane (for colder temperatures) as coolant. Reaction temperatures were monitored by calibrated thermocouple positioned within the reaction volume, and were controllable to within 0.5 K. Pressure control was achieved via a throttled vacuum pump connected to the reaction cell outlet; cell pressure was monitored by capacitance manometer. The flashlamp jacket, surrounding the reactant and cooling volumes, was filled with xenon to a pressure of approximately 30 Torr. The lamp was fired by discharge voltages from 20 to 25 kV, applied to tungsten electrodes at each end of the jacket, with typical discharge energies in the region of 600 J.

Analysis light was provided from 300 W xenon and 150 W deuterium lamps, the collimated outputs from which were coaligned using a dichroic beam splitter. The combined probe beam was passed through the reaction cell 8 times using White-type optics, giving a total absorption path length of 724 cm. A further dichroic reflector then split the beam into short (<250 nm) and long (> 250 nm) wavelength components. The short wavelength component was directed into a 0.5 m monochromator with 500 μm entrance slits (corresponding to a resolution of 0.5 nm fwhm), hereafter referred to as monochromator 1. The long wavelength component was divided using a beam splitter and directed into two further monochromators; a 0.3 m monochromator (150 μm slits, 0.3 nm fwhm resolution, monochromator 2) and a 0.25 m monochromator (150 μm slits, 0.3 nm fwhm resolution, monochromator 3).

During kinetic runs, monochromator 1 was used to monitor the formation of Cl_2O_2 at 210 nm, at which wavelength both ClO and Cl_2O made a minimal contribution to the total absorption (Figure 2). Monochromator 1 was also used to monitor photolytically induced absorption change at other wavelengths during the cross section measurement experiments, as described below. Monochromators 2 and 3 were set to monitor the maximum of the ClO ($\tilde{A}$, $v' = 12 \leftarrow \tilde{X}$, $v'' = 0$, $\Omega = 3/2$) band at 275.2 nm and the adjacent minimum at 276.4 nm—in practice the precise wavelength settings were tuned empirically to maximize and minimize (respectively) the measured ClO absorption signal. The proper alignment of the ClO detectors was confirmed by verifying that both channels returned the same absorption when tuned to the ClO (12,0) maximum.

All 3 monochromators were fitted with amplified photomultiplier tube detectors, the outputs from which were recorded and averaged using a 14-bit 100 kHz digital oscilloscope.

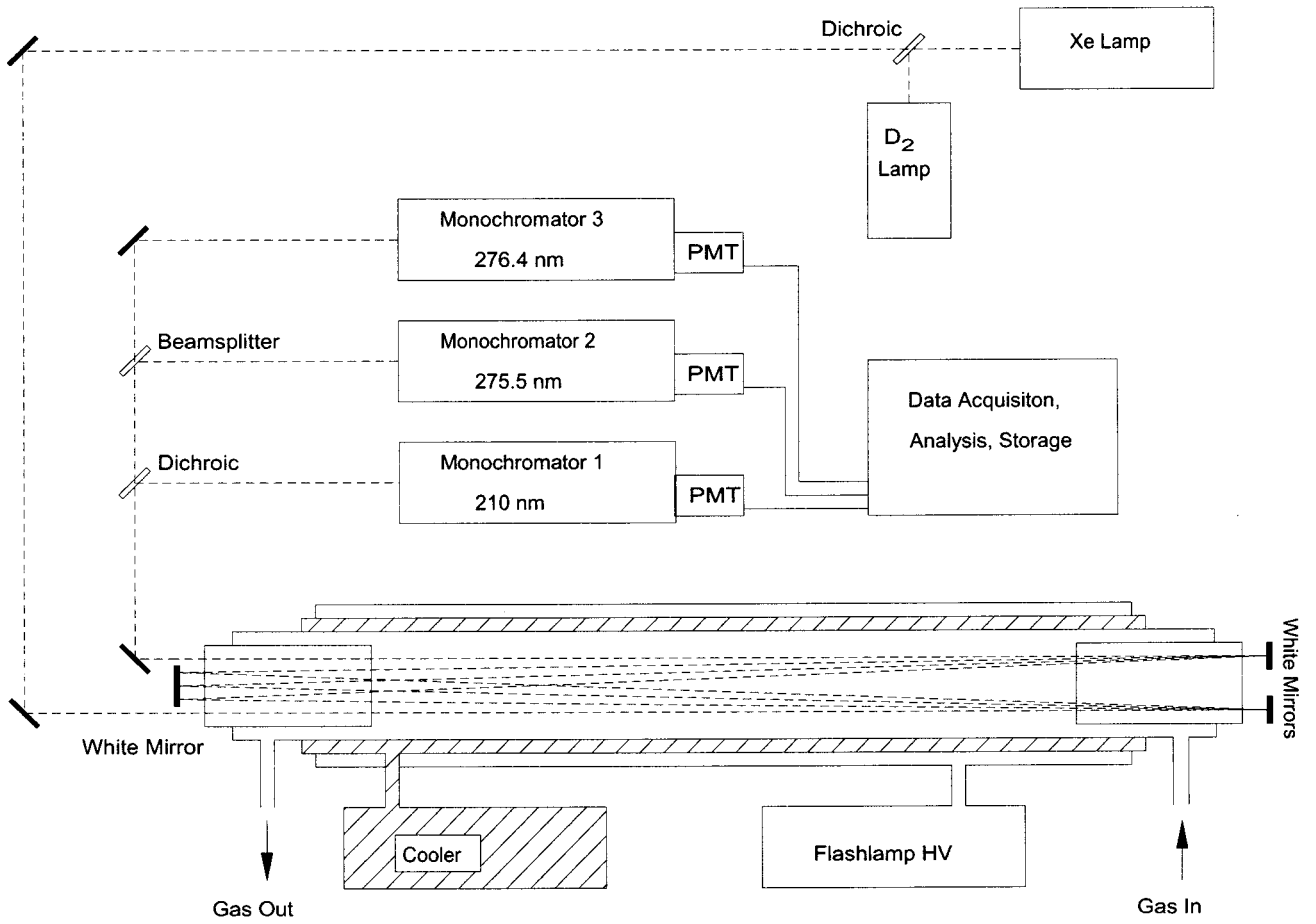

Figure 1. Schematic diagram of the experimental apparatus.

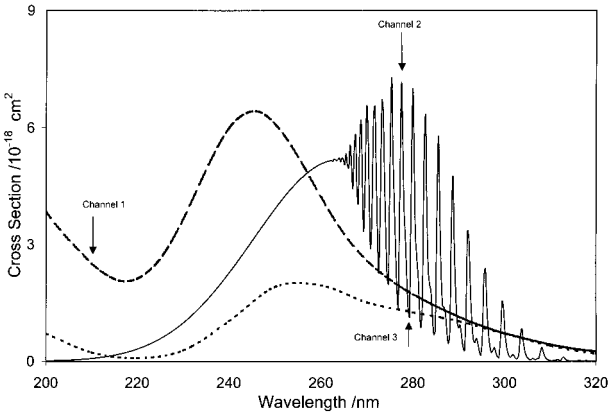

Figure 2. Absorption cross sections of ClO (solid line), Cl_2O_2 (dashed line) and Cl_2O (dotted line), showing the monitoring wavelengths used (210, 275.2, and 276.4 nm for channels 1, 2, and 3, respectively). Data from DeMore et al.[2]

Absorbance signals were typically analyzed after recording 50 to 100 shots. The absorption for each channel was obtained by evaluating $\ln(I_0/I_t)$, where I_0 represents the mean pre-photolysis signal and I_t the signal corresponding to time t following photolysis. The ClO differential absorption, $A_d(\mathrm{ClO})$, was then obtained by subtracting the absorption measured by channel 3 (276.4 nm) from that measured by channel 2 (275.2 nm)

$$A_d(\mathrm{ClO}) = \ln\left(\frac{I_0}{I_t}\right)_{\mathrm{Channel2}} - \ln\left(\frac{I_0}{I_t}\right)_{\mathrm{Channel3}} \qquad \text{(iv)}$$

The use of differential spectroscopy minimized the contribution to the measured ClO absorption due to the presence of other absorbing species: Over the small wavelength range between channels 2 and 3 (1.2 nm) the differential cross sections of the other species present (Cl_2O, Cl_2O_2 and Cl_2) were very small (less than 1−2% of that of ClO), and so correction for their presence made a negligible impact upon the determination of [ClO].

Reagent Preparation and Handling. Cl_2 (10% in He, 99.3%, Matheson) was used as supplied. Cl_2O was generated by passing Cl_2 over HgO according to the method of Cady.[25] Residual Cl_2 was removed by distillation at −108 °C. The Cl_2O sample was entrained in a flow of He through a bubbler held at dry ice temperature. N_2 (Air Products, 99.999%), O_2 (Air Products, 99.999%) and ClNO (Matheson) were used as supplied. NO (Matheson, 99%) was passed through an ascarite trap to remove excess NO_2. Br_2 (Aldrich, 99.5%) was purified through several freeze−pump−thaw cycles, and entrained in a flow of He through a bubbler maintained at 0 °C to ensure a known and convenient vapor pressure. OClO was generated online by passing Cl_2 (diluted to 1% in He) through an $NaClO_2$ column. Absorption measurements of the gas stream exiting the trap indicated that all the Cl_2 was converted to OClO when fresh sodium chlorite was used.

Radical Generation. For the principal kinetic experiments, ClO radicals were generated following the broadband photolysis of $Cl_2/Cl_2O/N_2$ mixtures

$$\mathrm{Cl_2} + h\nu \rightarrow 2\mathrm{Cl} \qquad (7)$$

$$\mathrm{Cl} + \mathrm{Cl_2O} \rightarrow \mathrm{Cl_2} + \mathrm{ClO} \qquad (8)$$

The concentrations employed (Cl_2, $1-5 \times 10^{15}$ molecules cm^{-3};

TABLE 3: Summary of the Four Independent σ_d(ClO) Measurements Performed

system	chemical scheme	calibrating cross section, σ_c	monitoring wavelength, nm
1	$Cl_2 + h\nu \rightarrow 2Cl$ $Cl + Cl_2O \rightarrow ClO + Cl_2$	$+ \sigma$ (ClO) $- \sigma$ (Cl_2O)	255
2	$OClO + h\nu \rightarrow ClO + O$	$- \sigma$ (OClO) (298 K) $- {}^1/_2\sigma$ (OClO) (204 K)	351 (298K), 409 (204K)
3	$Cl + Cl_2O \rightarrow ClO + Cl_2$ $Cl + NO + M \rightarrow ClNO + M$	$+ \sigma$ (ClNO)	220
4	$Br_2 + h\nu \rightarrow 2Br$ $Br + Cl_2O \rightarrow ClO + BrCl$	$+ \sigma$ (BrCl) $- {}^1/_2\sigma$ (Br_2)	366

Cl_2O, $1-2 \times 10^{14}$ molecules cm^{-3}, giving initial [ClO] $\approx 2-6 \times 10^{13}$ molecules cm^{-3}) were such that Cl atoms reacted rapidly with excess Cl_2O ensuring prompt ClO formation. Also, the Cl_2 concentration (considerably lower than that used by Hayman et al.[9] and Trolier et al.[12]) was such that the contribution to the ClO recombination rate arising from Cl_2 acting as a third body was always less than 3% of the total rate due to N_2-mediated reactions.

Kinetic experiments were performed as a function of pressure, between 15 and 700 Torr, at temperatures from 183 to 245 K. Experiments were performed as a function of [Cl_2] at each point in the (*T*, *P*) envelope. The 210, 275.2, and 276.4 nm absorbances were recorded at 200 μs intervals, for a total time period of approximately 0.1 s, with the flashlamp triggered after 7 ms. The resulting differential ClO and 210 nm absorption traces were analyzed using differential ClO cross sections to obtain absolute ClO and, hence, Cl_2O_2 concentrations, and so obtain kinetic and cross section data.

ClO Cross Sections. Absolute values for the differential ClO cross-section, σ_d(ClO), defined by

$$\sigma_d(\mathrm{ClO}) = \sigma(\mathrm{ClO}, 275.2\ \mathrm{nm}) - \sigma(\mathrm{ClO}, 276.4\ \mathrm{nm}) \quad \text{(v)}$$

are required to obtain rate coefficients for the second-order ClO self-reaction. In the case of structured regions of absorption spectra such as the halogen monoxide (A $\leftarrow$ *X*) transitions, absorption cross sections are dependent upon temperature and instrumental resolution and are also strongly sensitive to precise wavelength calibration. These factors complicate the use of cross sections from the literature measured upon different sets of experimental apparatus. The rate of a second-order reaction of this nature can therefore be most accurately determined using cross sections obtained *in situ*, under the precise optical conditions of the associated kinetic experiments. This approach was adopted in the current work.

Four independent methods were used for the determination of the ClO cross sections (as a function of temperature), summarized in Table 3. In each case, channel 1 was used to monitor the absorption change due to the consumption of the ClO precursor species or concomitant formation of some other product (permitting calibration of the ClO production), whereas channels 2 and 3 were used to monitor the differential ClO absorption, and the (wavelength) positions of these monochromators were maintained.

For each system, at each temperature, a series of experiments were performed corresponding to a range of initial ClO concentrations. The (differential) ClO absorption, A_d(ClO), and the associated calibrating absorption from channel 1, A_c, were measured immediately following photolysis (referred to hereafter as $t = 0$) for each experiment. σ_d(ClO) was then evaluated by linear regression of a plot of A_d(ClO) vs. A_c, in terms of the calibrating cross section, σ_c

$$A_d(\mathrm{ClO}) = \left(\frac{\sigma_d(\mathrm{ClO})}{\sigma_c}\right) \times A_c \quad \text{(vi)}$$

1. Cl + Cl$_2$O / 255 nm. ClO radicals were generated following the photolysis of $Cl_2/Cl_2O/N_2$ mixtures, in a manner analogous to the kinetic experiments. Monitoring channel 1 was used to determine the absorption change at 255 nm resulting from the consumption of Cl_2O and formation of ClO (the net production of Cl_2 made a negligible contribution (<0.02%) to the 255 nm absorption immediately following photolysis). At 255 nm, the absorption spectrum of ClO is smooth and hence resolution-independent; reference ClO cross sections from the literature can therefore be readily used to quantify ClO at this wavelength. The 255 nm absorption varied only slowly with respect to time, as this wavelength is close to the isobestic point [$\sigma(Cl_2O_2, 255\ \mathrm{nm}) \approx 2 \times \sigma(\mathrm{ClO}, 255\ \mathrm{nm})$], and was evaluated at $t = 0$. The value of A_d(ClO) at $t = 0$ was found via linear regression of a plot of $1/A_d$(ClO) vs time (ClO undergoing second-order decay). The differential ClO absorption was also evaluated in this way for systems 2 (at 300 K), 3 and 4.

The ClO 255 nm cross section used, 4.47×10^{-18} molecules^{-1} cm^2, was the mean of the determinations of Sander and Friedl[16] and Simon et al.[26] The Cl_2O cross section, 1.91×10^{-18} molecules^{-1} cm^2, was taken from the JPL 97−4 evaluation.[2] These values were applied at all temperatures. The 255 nm ClO cross section has been shown to be temperature independent.[12,18] The temperature dependence of $\sigma(Cl_2O, 255\ \mathrm{nm})$ was investigated by measuring the 255 nm absorption of a constant concentration (after correction for number density) of Cl_2O flowed through the reaction cell at temperatures between 197 and 300 K. The absorption, and hence $\sigma(Cl_2O, 255\ \mathrm{nm})$, was found to be constant (to within 10%) over this temperature range, in keeping with previous results.[21]

An example of the differential ClO and 255 nm absorption−time data is shown in Figure 3a (for 192 K), and the associated regression plot of A_d(ClO) vs A(255 nm) is shown in Figure 3b. The resulting values of σ_d(ClO) obtained at all temperatures are summarized in Table 4.

2. OClO + hν/351 and 409 nm. ClO radicals were generated following the photolysis of $OClO/N_2$ (300 K) or $OClO/O_2$ (204 K) mixtures. Channel 1 was used to quantify the loss of OClO, monitoring the most intense peak at 351.3 nm[27] at ambient temperature, and the less intense peak at 408.8 nm at 204 K. Approximate wavelength positioning of monochromator 1 was performed by reference to mercury line calibration; the monochromator was then tuned to the precise OClO band heads manually. The slits on monochromator 1 were set to 340 μm, giving a resolution of 0.25 nm to match that under which the reference OClO cross sections were measured.

At 294 K, ClO radicals were generated following the photolysis of OClO ($4-40 \times 10^{13}$ molecules cm^{-3}) in nitrogen

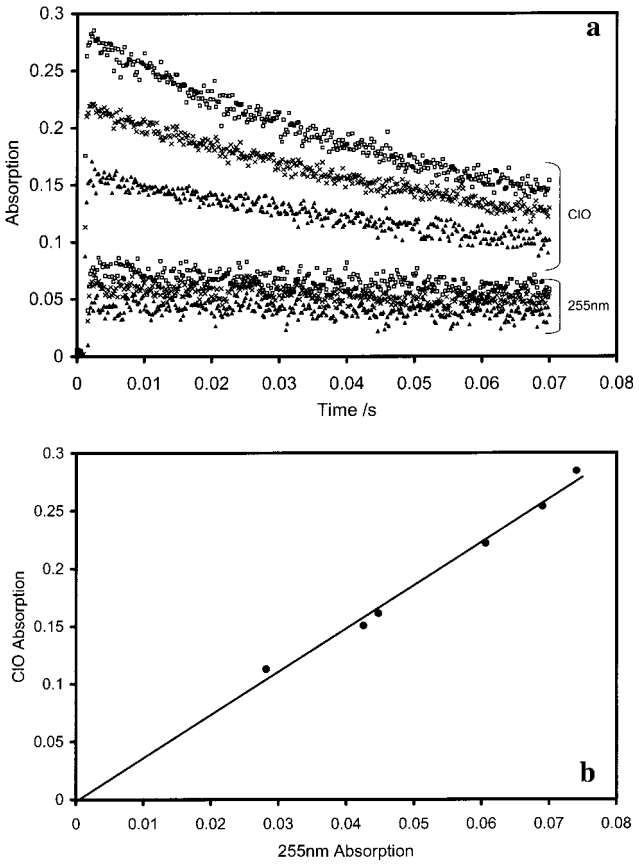

Figure 3. Example data for ClO cross section determination system 1, Cl + Cl_2O, obtained at 192 K: (a) ClO (differential) and 255 nm absorption − time data for various [Cl_2] (subset of data shown). (b) Linear regression of initial ClO and 255 nm absorptions.

bath gas. The subsequent rapid reactions of O and Cl atoms, reactions 10 and 11, lead to a unity quantum yield for ClO formation from OClO photolysis

$$OClO + h\nu \rightarrow O + ClO \qquad (9)$$

followed by either

$$O + ClO \rightarrow Cl + O_2 \qquad (10)$$

$$Cl + OClO \rightarrow ClO + ClO \qquad (11)$$

or

$$O + OClO \rightarrow O_2 + ClO \qquad (12a)$$

The resulting values of A_d(ClO) and A(OClO) were analyzed as described above (eq vi), using the determination of Wahner et al.[27] of σ(OClO, 351.3 nm) = 1.275×10^{-17} molecules^{-1} cm^2 for σ_c.

At 204 K, two further chlorine oxide association reactions occur to a significant extent

$$O + OClO + M \rightarrow ClO_3 + M \qquad (12b)$$

$$ClO + OClO + M \rightarrow Cl_2O_3 + M \qquad (13)$$

The formation of ClO_3 is negligible at higher temperatures (calculated to account for less than 1% of the O atoms formed from reaction 9 at 300 K) but at 204 K 10−20% of the O atoms would react to form ClO_3. As the stability and reactivity of ClO_3 is largely unknown,[28] and calculation of [ClO_3] formed would be critically dependent upon the rates of the O + ClO and O + OClO reactions, no correction for ClO_3 formation was attempted. Rather, O_2 was substituted for N_2 in the reaction mixture, leading to the near-exclusive (>99% at 200 Torr O_2) conversion of the O atoms to O_3. Cl_2O_3 formation via reaction 13 was negligible at 300 K, however k_{13} increases by a factor of 80 at 204 K, and the associated decomposition rate of Cl_2O_3 falls by a factor of 600.[2] As [OClO] ≫ [ClO], ClO underwent near exclusive (>98%) reaction with the (excess) OClO to form Cl_2O_3. The initial ClO concentration could thus be related to the final, $t = \infty$, change (relative to pre-photolysis) in OClO concentration as shown in eq vii

$$\Delta[OClO]_{t=\infty} = -2\Delta[ClO]_{t=0} \qquad (vii)$$

The 204 K data was thus analyzed using the values of $\Delta[OClO]_{t=\infty}$ for A_c in eq vi, with $\sigma_c = 2 \times \sigma$(OClO, 408.8 nm). σ(OClO, 408.8 nm) = 5.78×10^{-18} molecules^{-1} cm^2 at 204 K.[27] The resulting values of σ_d(ClO) obtained at 204 and 294 K are given in Table 4.

TABLE 4: Determinations of σ_d(ClO) as F(T)

T/K	σ_d(ClO)/10^{-18} molecules^{-1} cm^2
system 1: Cl_2O/255 nm	
352	4.20 ± 0.46
325	5.09 ± 0.92
296	4.92 ± 0.36
270	5.27 ± 2.12
245	6.53 ± 1.56
245[a]	6.12 ± 0.64
229	6.27 ± 0.67
213	8.01 ± 1.33
202	8.60 ± 1.92
192	9.60 ± 1.43
183	8.28 ± 1.24
system 2: OClO/351, 409 nm	
294	5.14 ± 0.20
204	8.01 ± 2.16
system 3: ClNO, 220 nm	
296	4.39 ± 0.32
245	6.29 ± 0.89
213	6.39 ± 0.73
192	8.46 ± 2.65
system 4: BrCl, 366 nm	
325	3.11 ± 1.75
296	3.39 ± 1.01
270	4.43 ± 0.39
256	3.46 ± 0.59
245	4.73 ± 0.50
234	4.34 ± 0.65
224	3.97 ± 2.52
213	5.48 ± 0.89
192	6.63 ± 1.49

[a] Errors are ±2σ; statistical only. [a]Second determination performed after all other measurements of σ_d(ClO).

3. Cl + Cl_2O / Cl + NO, 220 nm. In back-to-back experiments, the absorption due to ClO formation observed following the photolysis of $Cl_2/Cl_2O/N_2$ mixtures was compared with that due to ClNO formation following the photolysis of $Cl_2/NO/N_2$ mixtures. ClNO thus provided an actinometric calibration of Cl_2 photolysis/ClO production.

NO concentrations were such (ca. 4×10^{17} molecules cm^{-3}) that consumption of ClNO via reaction with Cl atoms (14, below) was minimal (in excess of 99.5% of the Cl atoms underwent reaction with NO). Subsidiary experiments indicated that under the conditions employed, thermal equilibration of Cl_2 and NO to form ClNO in the mixing line and reaction cell

TABLE 5: Reactions Employed in FACSIMILE Optimization Model

No.	reaction	rate coefficient expression
1	$Cl + Cl_2O \rightarrow Cl_2 + ClO$	$6.2 \times 10^{-11} \times \exp(130/T)$
2	$ClO + ClO \rightarrow Cl_2O_2$	optimized
3	$Cl_2O_2 \rightarrow ClO + ClO$	[a]
4	$ClO + ClO \rightarrow Cl_2 + O_2$	$1.0 \times 10^{-12} \times \exp(-1590/T)$
5	$ClO + ClO \rightarrow Cl + ClOO$	$3.0 \times 10^{-11} \times \exp(-2450/T)$
6	$ClO + ClO \rightarrow OClO + Cl$	$3.5 \times 10^{-13} \times \exp(-1370/T)$
7	$Cl + Cl_2O_2 \rightarrow Cl_2 + ClOO$	$7.6 \times 10^{-11} \times \exp(65.4/T)$ [b]
8	$Cl + OClO \rightarrow ClO + ClO$	$3.4 \times 10^{-11} \times \exp(160/T)$
9	$ClO + OClO \leftrightarrow Cl_2O_3$	[c]
10	$Cl + O_2 \leftrightarrow ClOO$	[c]

Units: molecules^{-1} cm^3 s^{-1} All rate constant expressions from DeMore et al.[2] (JPL 97−4) except [a]Cl_2O_2 thermal decomposition rate calculated in terms of the optimized association rate constant and the expression for K_{eq} from Sander et al.[14] (JPL 00−3). [b]T. Ingham, Private Communication. [c]Association and thermal decomposition rates calculated from expressions given by DeMore et al. (JPL 97−4)[2].

prior to photolysis was negligible (accounting for less than 1% of the total Cl_2).

ClNO formation was monitored at 220 nm, corresponding to the shoulder of the ClNO low wavelength band with σ(ClNO, 220 nm) = 8.96×10^{-18} molecule^{-1} cm^2.[29] At this wavelength, the NO cross section is less than 4×10^{-23} molecule^{-1} cm^2,[30] thus no significant spectral interference arose from the consumption of NO to form ClNO. The temperature dependence of the ClNO UV cross sections has only been reported for wavelengths longer than 350 nm.[31] The relative temperature dependence of the cross section at 220 nm was investigated by measuring the absorbance of ClNO samples in the reaction cell as a function of pressure, at various temperatures. Regression of the resulting absorption−pressure plots yielded the (relative) ClNO cross sections, when corrected for number density. Two sources of ClNO were used: A commercially supplied lecture bottle (Matheson), and a mixture of NO (12.5 Torr) and Cl_2 (5 Torr) diluted in a darkened bulb and allowed to equilibrate for several days. Absolute ClNO cross sections were not obtained due to limited precision in the various dilution stages. The value of σ(ClNO, 220 nm) (given as a function of temperature in Table 1S, Supporting Information), was found to decrease by approximately 30% between 300 and 190 K.

σ_d(ClO) was evaluated by performing experiments with either Cl_2O or NO as the Cl atom reaction partner as a function of [Cl_2], at a given temperature. Experiments were "sandwiched" alternating between NO and Cl_2O to confirm that the experimental conditions (e.g., photolysis flux) remained constant. The values of σ(ClNO, 220 nm) used for σ_c were obtained from the 298 K value reported by Tyndall et al.,[29] adjusted according to the relative temperature dependence given in Table 5. The resulting values of σ_d(ClO) obtained at 192, 213, 245, and 296 K are listed in Table 4.

4. Br + Cl$_2$O / 366 nm. ClO radicals were generated following the photolysis of Br_2 ($8 \times 10^{13} - 6 \times 10^{14}$ molecules cm^{-3}) in the presence of Cl_2O (ca. 7×10^{14} molecules cm^{-3}) and N_2 (balance to 25 Torr) mixtures, and quantified relative to the concomitant formation of BrCl

$$Br_2 + h\nu \rightarrow 2Br \quad (14)$$

$$Br + Cl_2O \rightarrow BrCl + ClO \quad (15)$$

Monitoring channel 1 was used to measure the absorption change at 366 nm arising from Br_2 loss and BrCl formation−366 nm corresponds to the maximum value of the quantity σ(BrCl) − $^1/_2\sigma(Br_2)$. Experiments were performed as a function of [Br_2], and σ_d(ClO) obtained as described above (eq vi), with $\sigma_c = \sigma(BrCl) - {}^1/_2\sigma(Br_2)$. The cross sections for BrCl and Br_2 at 366 nm, 3.84×10^{-19} and 1.36×10^{-19} molecules^{-1} cm^2 respectively at 298 K, were taken from Maric et al.[32]

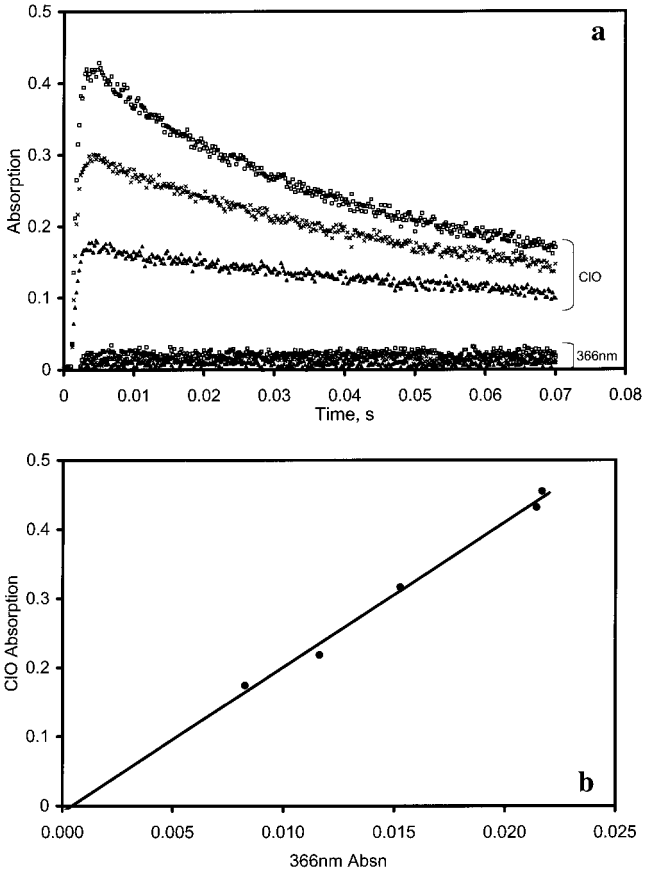

Figure 4. Example data for ClO cross section determination system 4, Br + Cl_2O, obtained at 200 K: (a) ClO (differential) and 366 nm absorption − time data for various [Br_2] (subset of data shown). (b) Linear regression of initial ClO and 366 nm absorptions.

Typical A_d(ClO) and A(366 nm) − time data from 192 K are shown in Figure 4a, with the accompanying regression shown in Figure 4b. The resulting values of σ_d(ClO) are given in Table 4.

Comparison of ClO Cross Section Determinations. The values of σ_d(ClO) listed in Table 4 are plotted in Figure 5, as a function of temperature. The determinations conducted using systems 1, 2, and 3 are in good agreement, while the results obtained using system 4 are consistently lower. The relative temperature dependencies of σ_d(ClO) obtained with (e.g.) systems 1 and 4 are in good agreement, indicating that the discrepancy between the systems is systematic in nature. The Cl_2O/255 nm cross section measurements (system 1) were performed before systems 2, 3, and 4; however, to verify the invariance of the experimental conditions throughout all the experiments a further 298 K determination was performed after the other measurements; this measurement, also given in Table 4, was in good agreement with the earlier determinations.

The BrCl system is the most chemically complex, with many possible secondary reactions occurring between the two halogen species present. BrCl cross sections at temperatures other than ambient are not available. The calibrating signal used in system 4, the absorption due to (BrCl − $^1/_2Br_2$), is the smallest by nearly an order of magnitude (System 1, Cl_2/Cl_2O: 2.56×10^{-18} molecule^{-1} cm^2; System 2, OClO, 1.275×10^{-17} molecule^{-1} cm^2; System 3, ClNO, 8.96×10^{-18} molecule^{-1} cm^2; System

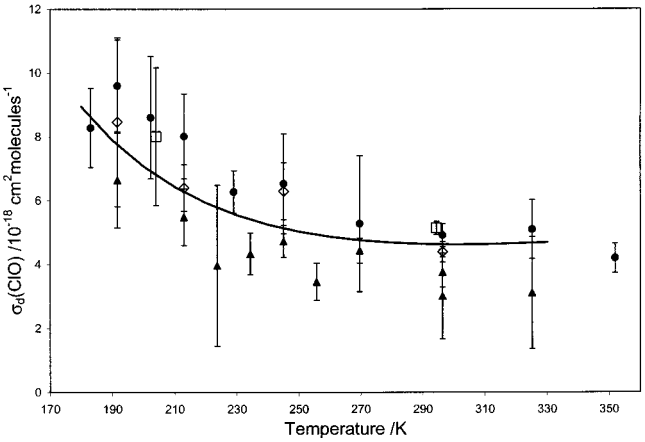

Figure 5. Values of σ_d(ClO) obtained as a function of temperature using system 1 (Cl + Cl_2O; filled circles), system 2 (OClO + $h\nu$; open squares), system 3 (Cl + Cl_2O or ClNO; open diamonds) and system 4 (Br + Cl_2O; filled triangles). Error bars are $\pm 2\sigma$ and represent precision only. Solid line is weighted fit of eq viii to all cross section determinations.

4, BrCl/Br_2, 3.16×10^{-19} molecule^{-1} cm^2) and hence is by far the most susceptible to both random errors (reflected in the greater scatter and error bars in Figure 4 for the results obtained from this system) and systematic errors arising from any underlying absorption of contaminants or unforseen secondary chemical effects. However, we were unable to unequivocally account for the discrepancy between the results from system 4 and those from systems 1, 2, and 3, thus all 4 sets of determinations were used to parametrize the temperature-dependent differential ClO cross sections, with the uncertainty (15%) propagated into the final kinetic results. The impact of this choice of ClO cross section upon the final results is discussed further below.

The temperature-dependence of σ_d(ClO) was parametrized according to eq viii, after Nickolaisen et al.[11]

$$\sigma_d(\mathrm{ClO})^T = \sigma_d(\mathrm{ClO})^{298} \times \left(a + \frac{b}{T} + \frac{c}{T^2}\right) \qquad \text{(viii)}$$

with $\sigma_d(\mathrm{ClO})^{298} = 4.63 \times 10^{-18}$ molecules^{-1} cm^2 and a, b, and c equal to 3.03, -1230, and 1.854×10^5 respectively; these values were obtained from a weighted fit to all the cross section data given in Table 4. This parametrization, also shown in Figure 5, was used to determine the kinetic results presented in the following section.

Kinetic Experiments: Analysis. The 210 nm and differential ClO absorption traces were analyzed using a model of the reaction system constructed in the kinetic simulation code FACSIMILE.[33] The model incorporated the principal reactions occurring, and simulated the contribution of all species to both of the measured absorption signals. The use of FACSIMILE permitted the simultaneous evaluation of k_{1a} and σ(Cl_2O_2, 210 nm), as contributions from ClO and Cl_2O to the time-dependent 210 nm absorption could be accounted for. The full reaction scheme used in the model is given in Table 5. Within the model, the values of $[Cl]_{t=0}$, the initial Cl atom concentration, and k_{1a} and σ(Cl_2O_2, 210 nm) were optimized to minimize the sum of squares of residuals between the observed and simulated absorption traces. A representative pair of decay traces and optimized fits are shown in Figure 6.

Deconvolution of the Cl_2O_2 absorption, and hence cross section, from the measured 210 nm absorption was contingent upon a knowledge of the ClO and Cl_2O absorption cross sections

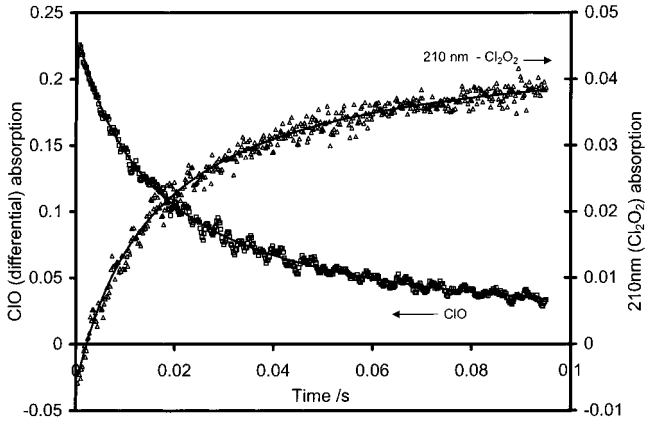

Figure 6. Typical ClO (open squares) and 210 nm (open circles) absorption−time data, together with optimized fits (solid lines). The negative values for the 210 nm absorption at short times arise due to the consumption of Cl_2O forming ClO radicals: The quantity shown is the photolytically induced *change* in absorption. Data shown for 202 K, 300 Torr.

at 210 nm. The value of 2.32×10^{-19} molecules^{-1} cm^2 was used for σ(Cl_2O, 210 nm), the mean of the three recently reported values (Lin,[34] 2.33; Molina and Molina,[35] 2.26; and Knauth et al.,[36] 2.38, all $\times 10^{-19}$ molecules^{-1} cm^2). No values for the 210 nm ClO cross sections have been reported; this parameter was derived from a subset of the absorption−time data sets: At very short times, the absorption (change) observed at 210 nm arose predominantly from the loss of Cl_2O and the formation of ClO, with very little Cl_2O_2 having yet formed (the 210 nm Cl_2 cross section is less than 10^{-25} molecules^{-1} cm^2 [37]). Thus, the decay traces at short times were sensitive to σ(ClO, 210 nm), the value of which was obtained via empirical optimization. σ(ClO, 210 nm) was evaluated for data sets obtained at pressures ranging from 100 to 700 Torr, in all cases the value returned being of the order of $(1.0 \pm 0.5) \times 10^{-19}$ molecule^{-1} cm^2. This level of uncertainty had a minimal impact upon the final values obtained for σ(Cl_2O_2, 210 nm): The sensitivity of the values obtained for k_{1a} and σ(Cl_2O_2, 210 nm) to the secondary reaction rates and the various cross sections employed in the optimization model is discussed below.

Results

ClO Self-Reaction Rate Coefficient. The optimized values of k_{1a} are given as a function of temperature, pressure and [Cl_2] in Table 2S (Supporting Information). No systematic variation was observed between the values of k_{1a} obtained (at a particular pressure and temperature) and the molecular chlorine concentration (which varied by a factor of 5), verifying that under the conditions employed in this work, Cl_2 made a negligible contribution to the ClO recombination rate. The falloff in the value of k_{1a} observed with bath gas pressure as the overall kinetics vary from third to second-order behavior was analyzed by fitting the data to the Troe-type falloff expression (eq i). In these fits, the value of the broadening factor, F_c, was fixed at 0.6, whereas the limiting low- and high-pressure limits for reaction 1a, k_0 and k_∞, were optimized. The fitting procedure was weighted according to the uncertainty in each value of k_{1a}. The resulting fits are shown in Figure 7, and the limiting low and high-pressure rate coefficients so obtained are listed in Table 6. The values of k_0 and k_∞ so obtained were parametrized according to equations (ii) and (iii), resulting in the values given below. The error limits represent the combined 2 standard deviation uncertainty from the fitting process and the systematic

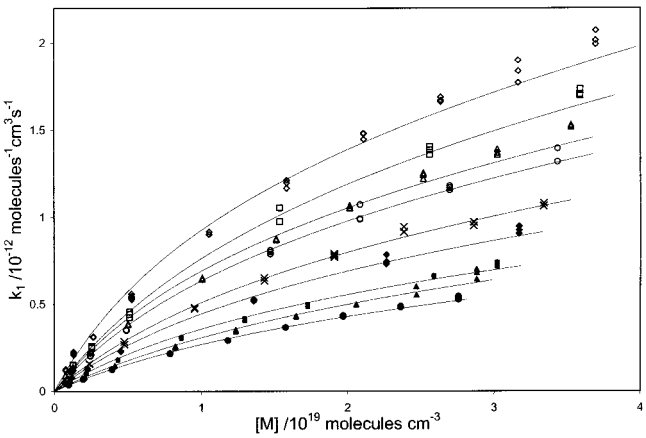

Figure 7. Measured values of k_{1a} (error bars omitted for clarity) and fitted falloff curves (eq i, using values from Table 6) as a function of total pressure and temperature: 183 K: open diamonds, 188 K: open squares, 192 K: open triangles, 197 K: open circles, 202 K: crosses, 213 K: filled diamonds, 224 K: filled squares, 234 K: filled triangles, and 245 K: filled circles.

TABLE 6: Limiting Low- and High-pressure Rate Coefficients for Reaction 1A

T/K	$k_0 \times 10^{32}$/ molecules^{-2} cm^6 s^{-1}	$k_\infty \times 10^{12}$/ molecules^{-1} cm^3 s^{-1}
183	17.6 ± 4.60	6.21 ± 0.55
188	12.70 ± 2.93	6.64 ± 0.87
192	11.15 ± 2.90	5.59 ± 0.57
197	10.86 ± 2.60	5.15 ± 0.60
202	8.79 ± 2.10	4.33 ± 0.43
213	7.52 ± 1.48	3.74 ± 0.46
224	6.07 ± 1.80	2.99 ± 0.34
234	4.69 ± 1.42	3.40 ± 0.43
245	4.22 ± 1.24	2.71 ± 0.33

Uncertainty represents combined statistical (2σ) and systematic uncertainty from ClO cross sections.

uncertainty inherent in the ClO cross sections

$$k_0 = (1.59 \pm 0.60) \times 10^{-32} \times (T/300)^{-4.50\pm0.98} \text{ molecules}^{-2}\,\text{cm}^6\,\text{s}^{-1} \quad \text{(ix)}$$

$$k_\infty = (1.36 \pm 0.22) \times 10^{-12} \times (T/300)^{-3.09\pm0.40} \text{ molecules}^{-1}\,\text{cm}^3\,\text{s}^{-1} \quad \text{(x)}$$

The temperature-dependent values of k_0 so obtained are compared with those from previous studies in Figure 8, discussed further below.

Cl_2O_2 Absorption Cross Section. The mean values obtained for the Cl_2O_2 absorption cross section at each temperature and pressure are shown in Figure 9. The cross section was found to be temperature independent, within the scatter of our results. The cross section was also found to be pressure independent at pressures of 100 Torr and above, and all data over this pressure range, at all temperatures, was averaged to obtain

$$\sigma(Cl_2O_2, 210\text{ nm}) = (2.94 \pm 0.86) \times 10^{-18}\text{ molecule}^{-1}\,\text{cm}^2$$

The uncertainty corresponds to the combined (2 standard deviations) statistical variation and the systematic uncertainty (15%) inherent in the ClO differential cross sections.

At pressures below 100 Torr, lower values for $\sigma(Cl_2O_2, 210$ nm) were obtained. The quality of the FACSIMILE fits to the 210 nm absorption traces was notably worse at the lowest

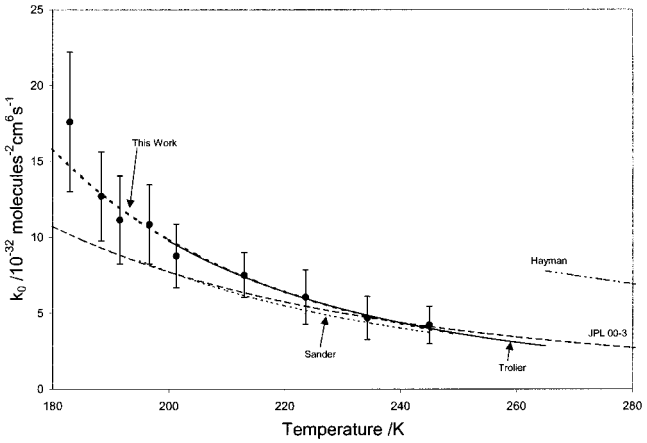

Figure 8. Comparison of temperature-dependent values of k_0 from this work (filled circles; fit = heavy dotted line) and previous studies: Hayman et al.: dashed/dotted line, Sander et al.: light dotted line, Trolier et al.: solid line (fit obtained without use of intercept), JPL 00−3 Evaluation: dashed line. Lines shown over temperature range of *kinetic* measurements.

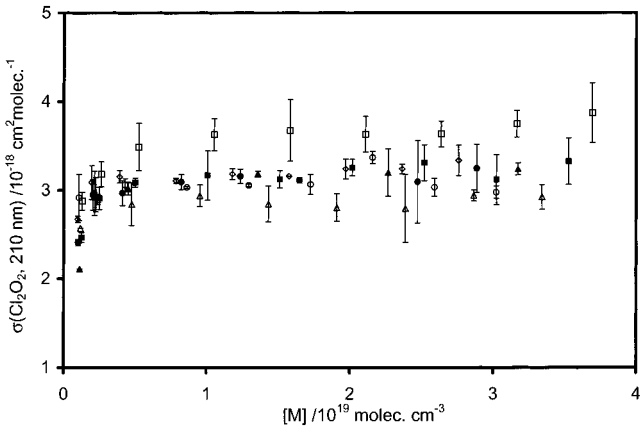

Figure 9. Measured 210 nm absorption cross sections of Cl_2O_2 as a function of temperature and pressure/number density: 183 K: open squares, 192 K: filled squares, 202 K:open triangles, 213 K: closed triangles, 224 K: open circles, 234 K: closed circles, and 245 K: open diamonds. Uncertainties are ± 2 s.d.

pressures (although those to the ClO decays were consistently excellent). The fits could be improved to some extent by reducing the 210 nm ClO absorption cross section used, which also slightly increased the returned value of $\sigma(Cl_2O_2, 210$ nm); however, even with σ(ClO, 210 nm) set to zero the fits were not as good as those obtained at higher pressures and the returned values of $\sigma(Cl_2O_2, 210$ nm) were somewhat lower, although within statistical (2 s.d.) agreement with the value given above.

Sensitivity Study. The sensitivity of the returned values of k_{1a} and $\sigma(Cl_2O_2, 210$ nm) to the secondary chemical reactions simulated in the reaction model (Table 6) was investigated by conducting multiple analyses of a representative data set, with the various model parameters varied sequentially up to their (2 s.d.) uncertainty limits, as assessed by DeMore et al.[2] The sensitivity to the kinetic parameters was found to be very low: The maximum changes in the returned values of k_{1a} and $\sigma(Cl_2O_2)$ for variation of any single rate coefficient in the model to the 2 standard deviation limit were 0.5 and 1.6% respectively. The insensitivity reflects the fact that under the conditions studied, formation of Cl_2O_2 was much faster than the bimolecular channels of the ClO self-reaction (i.e. $k_{1a}[M] \gg k_{1b} \approx k_{1c} \approx k_{1d}$). Thus, the bimolecular channels had very little

effect on ClO concentrations over the time scale of the ClO dimerization. Also, the decomposition of Cl_2O_2 is slow over the temperatures studied ($\leq$ 245 K); the 1/e lifetime of the dimer at 245 K is greater than 20 s.[11] Under these conditions the kinetics therefore reduced to simple second-order loss of ClO and formation of Cl_2O_2.

Similar sensitivity tests were performed to investigate the effect of varying the 210 nm cross sections used in the model for Cl_2O and ClO upon the returned value of the dimer cross section. The Cl_2O_2 cross section was found to be insensitive to the 210 nm Cl_2O cross section used: Variation of $\sigma(Cl_2O, 210\ nm)$ from 2.1 to 2.5 $\times$ 10^{-19} molecules^{-1} cm^2 (a range considerably greater than the uncertainty in this parameter) caused a variation in $\sigma(Cl_2O_2, 210\ nm)$ of less than 4%. The sensitivity of $\sigma(Cl_2O_2, 210\ nm)$ to $\sigma(ClO, 210\ nm)$ was somewhat greater, and dependent upon pressure: At pressures of 100 Torr and above, variation of up to 100% in $\sigma(ClO, 210\ nm)$ produced less than 5% change in the returned Cl_2O_2 cross section, whereas at the lowest pressures studied, the same variation lead to a 17% change in $\sigma(Cl_2O_2, 210\ nm)$. The changing sensitivity reflects the greater contribution of ClO (relative to Cl_2O_2) to the total 210 nm absorption at lower pressures over the time period studied, as the rate of reaction 1a is lower.

In summary, the model kinetics and ClO and Cl_2O 210 nm cross sections had a negligible effect upon the values of k_{1a} under all conditions and a minimal effect upon the values of $\sigma(Cl_2O_2)$ at pressures equal to and greater than 100 Torr. ClO underwent essentially pure second-order decay; accordingly, the returned value of k_{1a} was directly proportional to the value of $\sigma_d(ClO)$ used. The value obtained for $\sigma(Cl_2O_2, 210\ nm)$ was similarly dependent upon $\sigma_d(ClO)$, albeit with the dependence reduced by a factor of 2.

Discussion

ClO Differential Cross Section. No measurements of the temperature-dependence of the *differential* ClO cross sections have been reported in the literature. Measurements at the peak of the more intense vibronic bands of the A $\leftarrow$ *X* transition have been reported, between 220 and 450 K by Sander and Friedl[16] and between 200 and 298 K by Trolier et al.[12] However, as the deepening of the valleys and sharpening of the peaks of the ClO absorption make a comparable contribution to the temperature dependence of the cross section (at the broadly similar resolutions adopted in these studies, 0.2$-$0.3 nm fwhm) the literature results cannot be compared with this work. Maric and Burrows[37] have computed the ClO absorption spectrum as a function of temperature, and calculate the value of $\sigma_d(ClO)$ to increase monotonically from 4.8 to 7.9 $\times$ 10^{-18} molecule^{-1} cm^2 between 300 and 180 K. These values are in agreement (within uncertainty) with the results from this work, but do not aid our identification of the origin of the uncertainty in the cross section determinations reported here for the various systems. The discrepancies between the differential ClO cross section measurement systems may arise from two principal sources: The calibrating reference cross sections used and unforeseen secondary chemical interactions.

The reference cross sections used to quantify ClO production (Cl_2O and ClO at 255 nm, BrCl and Br_2 at 366 nm, OClO at 351 and 408 nm and ClNO at 220 nm) are the most significant potential source of systematic error in the determination of $\sigma_d(ClO)$, and hence of the discrepancy between the different chemical systems. The changes required to any single reference cross section to account for the difference between (e.g.) systems 1 and 4 (an increase of 37% in $\sigma(Cl_2O, 255\ nm)$, a reduction of $\sigma(ClO, 255\ nm)$ by 18%, an increase of $\sigma(BrCl, 366\ nm)$ by 32% or a reduction of $\sigma(Br_2, 366\ nm)$ of 178%) are all greater than the uncertainties in these parameters: Taking the spread of literature values as an indication of the accuracy with which each cross section is known, measurements of $\sigma(Cl_2O, 255\ nm)$[34,35,36] are in agreement to within 4%, and the measurements of $\sigma(ClO, 255\ nm)$ to within 10%. The 298 K measurements of $\sigma(BrCl, 366\ nm)$ by Seery and Britton[38] and by Maric et al.[32] agree to within 3%. Alternatively, a combination of smaller changes in the reference cross sections could account for the difference, with the maximum variation in any single parameter being 8%, comparable with the literature uncertainties (which, in the form quoted above, reflect principally the precision rather than the accuracy of the measurements).

Uncorrected secondary chemical interactions may also lead to errors in the determination of $\sigma_d(ClO)$. Of the four systems employed, we consider the Cl + Cl_2O (1) and Cl + NO (3) systems to be the least likely to be affected in this way, as in both cases the photolytically generated atom is rapidly and exclusively converted to ClO radicals and (relatively) unreactive molecular species. In the OClO system, the O atoms undergo competition for reaction between ClO and OClO, and termolecular formation of Cl_2O_3 and ClO_3 occurs at low temperatures. Although the conditions and analysis of these experiments were selected to account for these reactions, the more complex nature of the system enhances the potential for systematic error in the results. Similarly, the BrCl system involves the use of two halogen species, with considerable potential for unforseen secondary interactions involving various atom-molecule reactions and pre-photolysis equilibration. Principal among those which under the experimental conditions may lead to errors in the derived value of $\sigma_d(ClO)$ are the (possibly surface mediated) dark reaction of Br_2 and Cl_2O, potentially forming nascent BrCl prior to photolysis

$$Br_2 + Cl_2O \leftrightarrow 2BrCl + {}^1/_2O_2 \qquad (16)$$

(K_p, 298 K = 1.6 $\times$ 10^{18}). BrCl would photolyze very readily, and the subsequent reactions of Br and Cl atoms with Cl_2O would lead to ClO formation without (net) associated BrCl formation. The effect of these reactions would however be for $\sigma_d(ClO)$ to be overestimated, counter to the sense of the observed discrepancy.

The discrepancy in the values of $\sigma_d(ClO)$ obtained with the different chemical systems probably arises from a combination of unforseen secondary chemical interactions, potentially significant in the complex BrCl and (low temperature) OClO measurements, and minor inaccuracies in the reference cross sections used, exacerbated by the poor signal:noise ratio arising from the low calibrating absorption in the BrCl system. We consider the parametrization adopted (eq viii) to represent the temperature-dependent differential ClO cross sections at 0.3 nm fwhm resolution within our stated uncertainty of 15%.

Kinetics of ClO + ClO. The results obtained in this work are in good agreement with the measurements performed previously in this laboratory[10] (Figure 8). The values obtained for k_0 agree to within 8% over the temperature range in which both kinetic and cross sections measurements were performed in the earlier work (i.e., down to 220 K). At lower temperatures, higher values were obtained for the Cl_2O_2 formation rate coefficient in the present work. This discrepancy arises from the ClO cross sections used; in the previous study, these were extrapolated below 220 K using eq viii with $\sigma_d(ClO)^{298}$ = 8.4 $\times$ 10^{-18} molecule^{-1} cm^2, a = 1.011, b = $-$104.9 and c =

30330. Although this expression satisfactorily described the temperature-dependence of the ClO cross-section over the range of temperatures for which measurements of σ(ClO) were performed by Sander et al.[16] (220−400 K), the extrapolated values of σ(ClO) are not well constrained, particularly to lower temperatures where the quadratic dependence of σ(ClO) upon parameter c is greatest. This extrapolation probably underestimated the true values of σ(ClO) at temperatures below 220 K. Accordingly, the values of k_{1a} determined by Sander et al.[16] at the lowest temperatures were probably underestimated.

The falloff parametrization reported by Trolier et al.[12] which did not include an intercept is in excellent agreement with the results of this work (Figure 8). The alternative parametrization reported by Trolier et al. in which an intercept factor was added to the falloff curves is not shown in Figure 8 (as this does not reflect a directly comparable quantity to the other datasets), but corresponded to considerably lower values of k_0 than those obtained in this work at all temperatures. Trolier et al. commented that the apparent intercept in the measured rate (derived from the loss of ClO radicals) could be an artifact arising from complex falloff behavior if two isomers of Cl_2O_2 were to form. We did not observe any evidence for the existence of the intercept in the fall off curves at zero pressure (although our dataset included relatively few measurements at pressures below 50 Torr) indicating that such an intercept is not a feature of the basic ClO + ClO chemistry.

The invariance of the values of k_{1a} obtained in this work with respect to chlorine concentration and absence of any intercept in the falloff of k_{1a} at zero pressure (Figure 7) confirms that at the concentrations used ($1-5 \times 10^{15}$ molecules cm^{-3}) Cl_2 does not make a significant contribution to the ClO recombination rate, either through acting as a third body or via a chaperone mechanism.

Calculation of $k_{0,sc}$. The rate of third-order recombination reactions may be obtained following calculation of the rate of the corresponding unimolecular decomposition reaction through the equilibrium constant. Troe[39] has suggested a method for the calculation of such decomposition rate coefficients. This approach, as described by Patrick and Golden,[40] has been used to estimate the strong collision limiting low-pressure rate coefficient for reaction 1a, $k_{0,sc}$. This represents an upper limit for the observed weak collision rate coefficient, $k_{0,wc}$, related to the collision parameter β (by definition, $\beta \leq 1$)

$$k_{0,wc} = k_{0,sc} \times \beta \qquad \text{(xi)}$$

The input data used for the calculations and the results obtained are summarized in Table 7. The calculated value of $k_{0,sc}$ for reaction 1a at 200 K in N_2 is 4.5×10^{-32} molecules^{-2} cm^6 s^{-1}. This value is considerably lower than the (laboratory) results of this work (9.7×10^{-32}), the previous measurements of Trolier et al.[12] (9.8×10^{-32}), Sander et al.[10] (7.7×10^{-32}) and the JPL 00−3 evaluation[14] of 7.7×10^{-32} (all molecules^{-2} cm^6 s^{-1}).

Uncertainties in the calculated value of $k_{0,sc}$ arise particularly from the value of $\Delta_f H°$ (ClOOCl, 0 K) and the vibrational frequencies used. The enthalpy of formation of Cl_2O_2 has been determined experimentally (via van't Hoff analysis of K_{eq} measurements) by Cox and Hayman[19] and Nickolaisen et al.[11] to be 131 and 120.9 kJ mol^{-1} at 200−300 K, corresponding to values for $\Delta_f H°$(ClOOCl, 0 K) of 134.3 and 124.2 kJ mol^{-1} respectively. Lee et al.[41] performed an extensive *ab initio* study of the Cl_2O_2 isomers, and calculated a value of 143.1 kJ mol^{-1} for $\Delta_f H°$(ClOOCl, 0 K) with an estimated uncertainty of 7 kJ mol^{-1}. The mean value of these three determinations, 133.9 kJ mol^{-1}, was used in the calculation (Table 7). This value is in reasonably good agreement with the value from Chase et al.[42] (NIST-JANAF tables) of 136.5 ± 8 kJ mol^{-1} (obtained from the data of Cox and Hayman[19]); however, the uncertainty of ca. 10 kJ mol^{-1} corresponds to a range of values of $k_{0,sc}$ from 2.1×10^{-32} molecules^{-2} cm^6 s^{-1} (143.9 kJ mol^{-1}) to 8.9×10^{-32} molecules^{-2} cm^6 s^{-1} (123.9 kJ mol^{-1}).

TABLE 7: Input Data for Calculation of $k_{0,sc}$ (after Patrick and Golden[40])

frequencies, cm^{-1}	moments of inertia, g cm^2 × 10^{39}	T	$\Delta_f H°$, kJ mol^{-1}	$S°$, JK^{-1} mol^{-1}
750[a]	6.4270[d]	0	133.89	0
653[a]	35.2686[d]	200	130.67	271.45
560[a]	39.6879[d]			
438[b]				
329[b]				
127[c]				

Lennard−Jones parameters $\sigma(Cl_2O_2) = 1.18 \times V_b^{1/3}$ with $V_b = 61.2$ cm^{3}g^{-1}mol^{-1}, and $\epsilon/k(Cl_2O_2) = 1.21 \times T_b$ with $T_b = 280$ K (mean of Cl_2O and OClO boiling points). Vibrational frequencies from measurements of Burkholder et al.[18] [a]and Birk et al.[46] [c] and calculations of Lee et al.[41] [b]Moments of inertia from Chase et al.[42] (d). $\Delta_f H°$(0 K) used is mean of the values derived from measurements of Cox & Hayman[19] and Nickolaisen et al.[11] and calculated by Lee et al. Enthalpy and entropy data for ClO taken from Chase et al.[42] (NIST-JANAF). Entropy and enthalpy of formation for ClOOCl at 200 K calculated via statistical mechanics.

Similarly, the values obtained for $k_{0,sc}$ are strongly dependent upon the vibrational frequencies for ClOOCl: For example, reducing the two calculated frequencies, 438 and 329 cm^{-1} (Cl−O−O asymmetric and symmetric bend respectively) by 20% increases the calculated value of $k_{0,sc}$ by 47%. Thus, although the value initially calculated for $k_{0,sc}$ is lower than the value of $k_{0,wc}$ measured in several studies, the uncertainty in the input parameters for the calculation is such that the range of calculated values for $k_{0,sc}$ include and exceed all the measured values of $k_{0,wc}$. It appears unlikely, however, that the value of $k_{0,sc}$ is much greater than the values of $k_{0,wc}$ determined experimentally, indicating that if the discrepancy between experiment and theory can be reconciled through the uncertainties in the calculated parameters, the collision parameter β for reaction 1 in N_2 at 200 K is of the order of 0.8−1.

The calculation may be repeated for the alternative direct channel of reaction 1a forming ClOClO; taking frequencies, moments of inertia and enthalpies from Chase et al.[41] (as calculated by Lee et al.[41]) gives $k_{0,sc}$ (ClOClO) = 2×10^{-33} molecules^{-2} cm^6 s^{-1}, a factor of 10−40 lower than the value obtained for formation of ClOOCl. It is therefore unlikely that direct occurrence of this channel makes a significant contribution to the experimentally measured values of $k_{0,sc}$.

Cl_2O_2 Cross Section. The value obtained for the 210 nm Cl_2O_2 cross section ($(2.94 \pm 0.86) \times 10^{-18}$ molecule^{-1} cm^2) is approximately 17% higher than the JPL 97−4 evaluation[2] of 2.52×10^{-18} molecules^{-1} cm^2 (with an estimated uncertainty of ±50%); however the two values are in agreement within the uncertainty of our measurement. The origin of the apparently lower values of $\sigma(Cl_2O_2, 210\text{ nm})$ obtained at lower pressures (<100 Torr) in this work may lie in a combination of the ClO and Cl_2O 210 nm cross sections and the differential ClO cross sections used. However, as noted above, setting σ(ClO, 210 nm) to zero does not entirely remove this trend. The effect is ameliorated by reducing the value of σ_d(ClO); however, a reduction of 30% is required to reduce the difference between values of $\sigma(Cl_2O_2)$ measured at 25 Torr relative and those measured at 760 Torr to 5%. A reduction of σ_d(ClO) of this magnitude is inconsistent with all the ClO cross section determinations conducted in the course of this work.

Alternatively, the lower values may reflect a real change in the 210 nm absorption of the products of ClO + ClO, as formed in our reaction system, as a function of pressure. If two channels of the ClO + ClO association reaction occur, forming different isomers of Cl_2O_2 and exhibiting different kinetics/falloff behavior, the quantity measured as $\sigma(Cl_2O_2, 210\ nm)$ could arise from a combination of both isomers, formed in different proportions under different conditions, e.g., pressures. The possibility of ClO dimerizing to form the asymmetric dimer ClOClO has been considered previously, and indeed the observation of OClO + Cl as a major product channel of the reaction at higher temperatures indicates that one channel of the reaction proceeds through a ClOClO complex. However, ClOClO is calculated to be considerably less stable than ClOOCl. Of the isomers of Cl_2O_2, ClOOCl is the lowest lying with the T-shaped isomer $ClClO_2$ and the asymmetric dimer ClOClO lying approximately (3.8 ± 8.2) and (42 ± 17) kJ mol^{-1} higher in energy respectively (at 0 K; from Lee et al.[41]). Direct formation of $ClClO_2$ is unlikely, however it has been suggested[43] that ClOClO could isomerize to the more stable $ClClO_2$ isomer

$$ClO + ClO + M \leftrightarrow ClOClO + M \qquad \Delta_r H\ (298\ K) = -27\ kJ\ mol^{-1} \quad (17)$$

$$ClOClO\ (+M?) \rightarrow ClClO_2\ (+M?) \qquad \Delta_r H\ (298\ K) = -40\ kJ\ mol^{-1} \quad (18)$$

(Enthalpies from ref 41). The 210 nm absorption cross section of $ClClO_2$ has been found to be 7.5×10^{-18} molecules^{-1} cm^2 (Müller and Willner[44]) and 8.3×10^{-18} molecules^{-1} cm^2 (Jacob et al.[45]). These values are considerably greater than the ClOOCl cross section at 210 nm (2.52×10^{-18} molecules^{-1} cm^2). Even a minor channel of the ClO + ClO reaction into $ClClO_2$ would lead to a considerable increase in the measured absorption at 210 nm compared to that observed if ClOOCl were the exclusive product.

Occurrence of reactions 17 and 18 in addition to reaction 1a could lead to a complex pressure-dependence of the branching ratio for formation of the various Cl_2O_2 isomers; for example, collisional enhancement of the isomerization of ClOClO in competition with dissociation back to 2 ClO radicals could lead to greater yields of $ClClO_2$ at higher pressures. The apparent increase in the value of $\sigma(Cl_2O_2, 210\ nm)$ with pressure observed in this work could then reflect changing fractional production of $ClClO_2$ and ClOOCl as final products of the ClO + ClO reaction, with production of ClOOCl dominating at low pressures and a minor channel leading to $ClClO_2$ formation manifest at higher pressures. A 7% yield of $ClClO_2$ with a cross section of 8.3×10^{-18} rather than ClOOCl (2.5×10^{-18}) would result in an apparent Cl_2O_2 cross section of 2.9×10^{-18} (all molecules^{-1} cm^2).

Birk et al.[46] have measured the rotational spectrum of Cl_2O_2, and deduced that chlorine peroxide ClOOCl was the dominant product of reaction 1a. They used a microwave discharge to generate Cl atoms which were reacted with Cl_2O to form ClO, which underwent self-reaction to form ClOOCl in a reaction chamber held at 10 Torr total pressure, before passing through the absorption cell at 100 mTorr. Under these conditions, little if any $ClClO_2$ might be expected to form via the mechanism above, depending upon the relative rates of reactions 1a, 17, and 18. Similarly, the measurements of $\sigma(Cl_2O_2)$ performed by Burkholder et al.[18] used pre-reactor pressures of 25−35 Torr and absorption cell pressures of 10 Torr to generate and monitor Cl_2O_2. The experiments of Cox and Hayman,[19] and the repeated measurements of DeMore and Tschuikow-Roux[21]/Huder and DeMore[22] were performed under very different conditions and time scales; Cox and Hayman used 1 atm of nitrogen and time scales of the order of 60 s, whereas the DeMore et al. experiments were conducted in 2−3 atm of nitrogen or the cryogenic solvents N_2O, CO_2, and CF_4, over time scales of up to 7 min. Although the higher pressures of these experiments might be expected to favor $ClClO_2$ formation according to the kinetic scheme conjectured above, the larger time scale of these experiments may facilitate formation of ClOOCl.

Further experiments investigating the formation of ClOOCl over time scales and pressures intermediate to those thus far performed could verify whether reactions 17 and 18 occur to any significant extent, or if the apparent trend in the value for $\sigma(Cl_2O_2, 210\ nm)$ with pressure obtained in the present work is an artifact introduced through cumulative inaccuracies in the various reference cross sections employed in the optimization model. The flash photolysis technique as applied in this work is not ideally suited to such studies, as wall losses and flowout dominate chemistry in determining reactant concentrations at time scales above a few tenths of a second.

Atmospheric Implications. The presence of oxygen in the atmosphere necessitates correction of the expression for k_0 to account for the differing third body efficiencies of O_2 and N_2 in reaction 1a. The relative efficiency for M = O_2 relative to M = N_2 for ClO dimerization has been found to be 0.62 (Nickolaisen et al.[11]) to 0.82 (Trolier et al.[12]). Taking the mean of these two measurements the rate coefficient for reaction 1a should be reduced by 6% for M = 0.21 O_2/0.79 N_2 relative to M = N_2, i.e., (to a first approximation)

$$k_{0(atm)} = (1.49 \pm 0.56) \times 10^{-32} \times (T/300)^{-4.50 \pm 0.98}\ molecules^{-2}\ cm^6\ s^{-1} \quad (xii)$$

Our results indicate that the ClO self-reaction rate coefficient is larger than that given in the JPL 00−3 (Sander et al.[14]) evaluation for pressures and low temperatures typical of the polar stratosphere: At a pressure of 50 mbar, the ratio of k_{1a} from the present study to the JPL 00−3 value is 1.39, 1.31, and 1.21 at temperatures of 180, 190, and 200 K, respectively. The calculated rate of destruction of atmospheric ozone by the ClO + ClO catalytic cycle (reactions 1−4) will therefore increase.

Numerous previous studies, using various approaches and data sets to define "measured" and "modeled" rates of chemical ozone loss, conclude that chemical loss of polar ozone in the Arctic occurs more rapidly than expected on the basis of the JPL 00−3 kinetic parameters (e.g., Bregman et al.,[47] Hansen et al.,[48] Becker et al.,[49] Woyke et al.,[50] Becker et al.[51]). However, an analysis of UARS MLS measurements of ClO and O_3 concentrations shows good agreement between measured and modeled chemical ozone loss rates for the Antarctic during 1992, 1993 and 1994 using JPL 00−3 kinetics (Wu and Dessler[52]). The reasons for this apparent discrepancy are unclear. Nonetheless, a faster rate for reaction 1 would lead to better agreement between measured and modeled rates of ozone loss for the majority of the recently published studies.

To evaluate the impact of our value for k_{1a} upon calculated ozone destruction rates, it is important to distinguish between studies which base modeled loss rates on measurements of [ClO] (e.g., Wu and Dessler) and studies which base modeled loss rates on calculated [ClO]. Typically, calculated [ClO] is determined using either lagrangian trajectory simulations[49] or 3-dimensional general circulation model simulations. For the

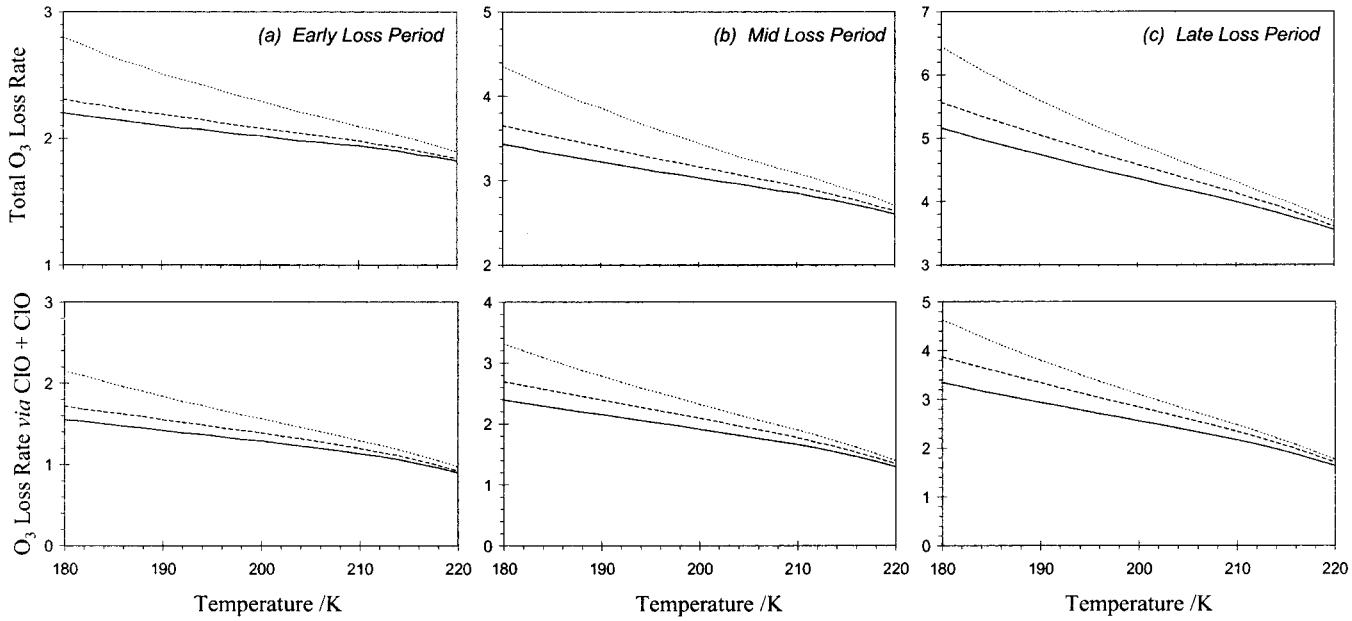

Figure 10. Model results: 24 h averaged ozone loss rates for 70°S, 50 mbar as a function of temperature. Three periods during the austral winter/spring are considered: (a) Early Antarctic ozone loss: Dec = 10°; ClO_x = 3 ppb, BrO_x = 10 ppt; O_3 = 3 ppm. (b) Mid Antarctic ozone loss: Dec = 5°; ClO_x = 2.4 ppb, BrO_x = 10 ppt; O_3 = 2 ppm. (c) Late Antarctic ozone loss: Dec = 0°; ClO_x = 1.6 ppb, BrO_x = 10 ppt; O_3 = 1 ppm. For each scenario, the lower panel gives the ozone loss rate, in percent per day, due to the ClO + ClO cycle, and the upper panel the total ozone loss rate. Solid Lines: JPL 00−3 Kinetics. Dotted Lines: Our value for k_{1a} with [ClO] fixed (case 1). Dashed Lines: Our value for k_{1a} with [ClO_x] fixed (case 2).

studies which base modeled ozone loss rates on measured [ClO], the rate of loss due to the ClO + ClO cycle will scale in proportion to the ratio R, given by

$$R = k_{1a}\,(\text{this work})/k_{1a}\,(\text{JPL } 00-3) \qquad \text{(xiii)}$$

and the loss rates due to other catalytic cycles involving ClO will be unaffected by the change in k_{1a}. However, for studies which base modeled loss rates on calculated [ClO], the increase in the rate of ozone loss due to the ClO + ClO cycle will be less than R: A higher value for k_{1a} will alter the ClO_x (= ClO + 2 × Cl_2O_2) partitioning from ClO into Cl_2O_2, reducing [ClO]. The product $2k_{1a}[ClO]^2$, which limits the rate of ozone loss via the ClO + ClO cycle under cold conditions (i.e., when the photolysis rate of Cl_2O_2 greatly exceeds its thermal decomposition rate) will therefore rise by less than the increase in k_{1a}. Moreover, the reduction in [ClO] due to the increase in k_{1a} will lower the rate of ozone loss through the ClO + BrO and ClO + O cycles.

A simple numerical model[53] was employed to estimate the effect of the present laboratory measurement of k_{1a} on the ozone destruction rate in the polar stratosphere for both classes of model studies described above. The model used in these calculations simulates the evolution of an isolated air parcel at specified conditions of [ClO_x], [BrO_x] (= BrO + BrCl) and solar declination. Photolysis frequencies are calculated at each zenith angle using climatological values of the overhead ozone and an albedo that is consistent with polar conditions. Results are obtained by integrating the rate equations until steady-state over a 24 h period is achieved. Two types of calculations were performed: In the first case (I), the model was constrained by a specified value of [ClO] versus solar zenith angle. In the second case (II), the model was constrained by a specified value of total reactive chlorine (ClO_x) and the partitioning of species within the ClO_x family was allowed to vary in response to variations in k_{1a}.

The model was used to investigate the effect of changes in k_{1a} upon 24-hour averaged ozone loss at a latitude of 70° S and a pressure of 50 mbar for three periods, representative of "early", "mid", and "late" episodes of ozone loss during a typical austral winter/spring. Model results are shown in Figure 10(a−c); see caption for a detailed description of the model constraints. In each figure, the top panel shows the total ozone loss rate, and the bottom panel the loss rate due to the ClO + ClO cycle. In each panel, the solid line shows the ozone loss rate calculated using JPL 00−3 kinetics, the dotted line shows the loss rate calculated using our value for k_{1a} with [ClO] fixed (case I) and the dashed line shows the loss rate calculated using our value for k_{1a} with [ClO_x] fixed (case II).

The model calculations show that for case I (fixed ClO) the value of k_{1a} reported here leads to an increase in the total ozone loss rate (relative to that calculated using JPL 00−3 kinetics) of up to 28%. The ozone loss rate due to the ClO + ClO cycle rises by up to 40%, directly reflecting the change in k_{1a}. The temperature dependence of the change in loss rate for this simulation reflects the temperature dependence of the ratio R (equation xiii); the largest effects are seen for cold air parcels ($T \approx 180$ K). The impact of our measured value for k_{1a} upon ozone loss rates is considerably smaller for case II (fixed [ClO_x]). In this simulation, the total loss rate rises by only about 8% for the coldest air parcels considered over the "late" loss period. The buffering of ClO to Cl_2O_2 partially counteracts the increase in k_{1a}, and the resulting reduction in [ClO] lowers the ozone loss rate through the ClO + BrO and ClO + O cycles.

These calculations illustrate that the impact of our measured value of k_{1a} upon our understanding of polar ozone loss rates will be largely dependent upon the type of model calculation which is used to "compare" to measured ozone loss rates. Increasing k_{1a} will have a considerably larger impact in models which are tied to measured [ClO] than in models which calculate [ClO] from first principles. There are merits to both approaches. The discrepancy between measured and modeled ozone loss rates, for models studies which calculate [ClO] from first principles, is in general larger than the increase in total loss rate that will be found by adopting our value for k_{1a}. Thus,

although an increase in k_{1a} pushes model results in the right direction, it is unlikely to be the sole explanation for the discrepancy noted for this class of model studies. Finally, we note that use of our value of k_{1a} in model studies tied to measured [ClO] will not only increase the calculated ozone loss rate, but will also result in a considerable increase in the calculated value of $[Cl_2O_2]$. A full exploration of the impact of a larger value for k_{1a} on our understanding of polar ozone will require considerable future analysis.

Summary

The rate coefficient for the formation of Cl_2O_2 from the self-reaction of ClO radicals has been measured over the range of conditions relevant to the polar stratosphere, and found to be in agreement with the current evaluation at the higher temperatures common to previous studies ($T \geq$ ca. 200−220 K); however, at lower temperatures the rate has been found to be higher than extrapolation of the previous results suggests. The limiting low- and high-pressure rate coefficients for reaction 1 in nitrogen have been determined to be $k_0 = (1.59 \pm 0.60) \times 10^{-32} \times (T/300)^{-4.50\pm0.98}$ molecules^{-2} cm^6 s^{-1} and $k_\infty = (1.36 \pm 0.22) \times 10^{-12} \times (T/300)^{-3.09\pm0.40}$ molecules^{-1} cm^3 s^{-1} respectively, obtained with $F_c = 0.6$. The corresponding value for k_0 in air is $k_{0(atm)} = (1.49 \pm 0.56) \times 10^{-32} \times (T/300)^{-4.50\pm0.98}$ molecules^{-2} cm^6 s^{-1}. The 210 nm absorption cross section of Cl_2O_2 has been measured following time-resolved monitoring of its formation via ClO radical association, and a mean value of $(2.94 \pm 0.86) \times 10^{-18}$ molecule^{-1} cm^2 obtained, temperature independent (to within ± 15%) between 183 and 245 K.

Acknowledgment. The research described in this paper was carried out at the Jet Propulsion Laboratory, California Institute of Technology under contract to the National Aeronautics and Space Administration. The authors thank D.B. Natzic for technical assistance.

Supporting Information Available: Table 1S, relative ClNO cross sections measured at 220 nm as a function of temperature, and Table 2S, the measured bimolecular ClO self-reaction rate coefficients listed as a function of temperature, pressure and molecular chlorine concentration. This information is available free of charge via the Internet at http://pubs.acs.org.

References and Notes

(1) *Scientific Assessment of Ozone Depletion: 1998*, World Meterological Organisation Global Ozone Research and Monitoring Project, Report No. 44, Geneva, **1999**.

(2) DeMore, W. B.; Sander, S. P.; Golden, D. M.; Hampson, R. F.; Kurylo, M. J.; Howard, C. J.; Ravishankara, A. R.; Kolb, C. E.; Molina, M. J. *Chemical Kinetics and Photochemical Data for use in Stratospheric Modelling*, Evaluation No. 12, JPL Publication 97-4, Jet Propulsion Laboratory, Pasadena, CA, 1997.

(3) Porter, G. *Proc. R. Soc. London A* **1950**, *200*, 284.

(4) Porter, G.; Wright, F. J. *Discuss. Faraday Soc.* **1953**, *14*, 23.

(5) Johnston, H. S.; Morris, E. D.; Van den Bogaerde, J. *J. Am. Chem. Soc.* **1969**, *81*, 7712.

(6) Cox, R. A.; Derwent, R. G. *J. Chem. Soc. Faraday Trans. I* **1979**, *75*, 1635.

(7) Cox, R. A.; Derwent, R. G.; Eggleton, A. E. J.; Reid, J. H. *J. Chem. Soc. Faraday Trans. I* **1979**, *75*, 1648.

(8) Molina, L. T.; Molina, M. J. *J. Phys. Chem.* **1987**, *91*, 433.

(9) Hayman, G. D.; Davies, J. M.; Cox, R. A. *Geophys. Res. Lett.* **1986**, *13*, 1347.

(10) Sander, S. P.; Friedl, R. R.; Yung, Y. L. *Science* **1989**, *145*, 1095.

(11) Nickolaisen, S. L.; Friedl, R. R.; Sander, S. P. *J. Phys. Chem.* **1994**, *98*, 155.

(12) Trolier, M.; Mauldin, R. L., III; Ravishankara, A. R. *J. Phys. Chem.* **1990**, *94*, 4896.

(13) Troe, J. *J. Phys. Chem.* **1983**, *83*, 114.

(14) Sander, S. P.; Friedl, R. R.; DeMore, W. B.; Golden, D. M.; Kurylo, M. J.; Hampson, R. F.; Huie, R. E.; Moortgat, G. K.; Ravishankara, A. R.; Kolb, C. E.; Molina, M. J. *Chemical Kinetics and Photochemical Data for use in Stratospheric Modelling*, Supplement to Evaluation No. 12, JPL Publication 00-3, Jet Propulsion Laboratory, Pasadena, CA, **2000**.

(15) Clyne, M. A. A.; Coxon, J. A. *Proc. R. Soc. A* **1968**, *303*, 207.

(16) Sander, S. P.; Friedl, R. R. *J. Phys. Chem.* **1989**, *93*, 4764.

(17) Basco, N.; Hunt, J. E. *Int. J. Chem. Kinet.* **1979**, *61*, 649.

(18) Burkholder, J. B.; Orlando, J. J.; Howard, C. J. *J. Phys. Chem.* **1990**, *94*, 687.

(19) Cox, R. A.; Hayman, G. D. *Nature* **1988**, *332*, 796.

(20) Permien, T.; Vogt, R.; Schindler, R. N. p 149 in *Air Pollution Report No. 17*, R. A. Cox, Ed., Commision of the E. C., Brussels, **1988**.

(21) DeMore, W. B.; Tschuikow-Roux, E. *J. Phys. Chem.* **1990**, *94*, 5856.

(22) Huder, K. J.; DeMore, W. B. *J. Phys. Chem.* **1995**, *99*, 3905.

(23) Watson, R. T.; Sander, S. P.; Yung, Y. L. *J. Phys. Chem.* **1979**, *83*, 2936.

(24) Nickolaisen, S. L.; Roehl, C. M.; Blakeley, L. K.; Friedl, R. R.; Francisco, J. S.; Liu, R.; Sander, S. P. *J. Phys. Chem.* **2000**, *104*, 308.

(25) Cady, G. H. *Inorg. Synth.* **1967**, *5*, 156.

(26) Simon, F. G.; Schneider, W.; Moortgat, G. M.; Burrows, J. P. *J. Photochem. Photobiol. A: Chem.* **1990**, *55*, 1.

(27) Wahner, A.; Tyndall, G. S.; Ravishankara, A. R. *J. Phys. Chem.* **1987**, *91*, 2734.

(28) Collussi, A. J.; Sander, S. P.; Friedl, R. R. *J. Phys. Chem.* **1992**, *96*, 4442.

(29) Tyndall, G. S.; Stedman, K. M.; Schneider, W.; Burrows, J. P.; Moortgat, G. K. *J. Photochem.* **1987**, *36*, 133.

(30) Thompson, J. *J. Geophys. Res.* **1963**, *68*, 6431.

(31) Roehl, C. M.; Orlando, J. J.; Calvert, J. G. *J. Photochem. Photobiol. A: Chem.* **1992**, *69*, 1.

(32) Maric, D.; Burrows, J. P.; Moortgat, G. K. *J. Photochem. Photobiol. A: Chem.* **1994**, *83*, 179.

(33) Curtis, A. R.; Sweetenham, W. P. FACSIMILE, AERE Harwell publication R 12805, Computer Science and Systems Division, Harwell Laboratory, Oxfordshire, U.K. **1987**.

(34) Lin, C. L. *J. Chem. Eng. Data* **1976**, *21*, 411.

(35) Molina, L. T.; Molina, M. J. *J. Phys. Chem.* **1978**, *82*, 2410.

(36) Knauth, H. D.; Alberti, H.; Clausen, H. *J. Phys. Chem.* **1979**, *83*, 1604.

(37) Maric, D.; Burrows, J. P.; Meller, R.; Moortgat, G. K. *J. Photochem. Photobiol. A: Chem.* **1993**, *70*, 205.

(38) Seery, D. J.; Britton, D. *J. Phys. Chem.* **1964**, *68*, 2263.

(39) Troe, J. *J. Chem. Phys*. **1977**, *66*, 4745 and *J. Chem. Phys*. **1977**, *66*, 4758.

(40) Patrick, R.; Golden, D. M. *Int. J. Chem. Kinet.* **1983**, *15*, 1189.

(41) Lee, T. J.; Rohlfing, C. M.; Rice, J. E. *J. Chem. Phys.* **1992**, *97*, 6593.

(42) Chase, M. W, Ed. *J. Phys. Chem. Ref. Data* **1998**, *9*, 844.

(43) McGrath, M. P.; Clemitshaw, K. C.; Rowland, F. S.; Hehre, W. J. *J. Phys. Chem.* **1990**, *94*, 6126.

(44) Müller, H. S. P.; Willner, H. *Ber. Bunsen-Ges. Phys. Chem.* **1992**, *96*, 427.

(45) Jacobs, J.; Kronberg, M.; Müller, H. S. P.; Willner, H. *J. Am. Chem. Soc.* **1994**, *116*, 1106.

(46) Birk, M.; Friedl, R. R.; Cohen, E. A.; Pickett, H. M.; Sander, S. P. *J. Chem. Phys.* **1989**, *91*, 6588.

(47) Bregman, A., van den Broek, M.; Carslaw, K. S.; Muller, R.; Peter, T.; Scheele, M. P.; Lelieveld, J. *J. Geophys. Res.* **1997**, *102*, 10815.

(48) Hansen, G.; Svenoe, T.; Chipperfield, M. P.; Dahlback, A.; Hoppe, U. P. *Geophys. Res. Lett.* **1997**, *24*, 799.

(49) Becker, G.; Muller, R.; McKenna, D. S.; Rex, M.; Carslaw, K. S. *Geophys. Res. Lett.* **1998**, *25*, 4325.

(50) Woyke, T.; Muller, R.; Stroh, F.; McKenna, D. S.; Engel, A.; Margitan, J. J.; Rex, M.; Carslaw, K. S. *J. Geophys. Res.* **1999**, *104*, 18 755.

(51) Becker, G.; Muller, R.; McKenna, D. S.; Rex, M.; Carslaw, K. S.; Oelhaf, H. *J. Geophys. Res.* **2000**, *105*, 15 175.

(52) Wu, J.; Dessler, A. E. *J. Geophys. Res.* **2001**, *106*, 3195.

(53) Salawitch, R. J.; Wofsy, S. C.; Gottlieb, E. W.; Lait, L. R.; Newman, P. A.; Schoeberl, M. R.; Loewenstein, M.; Podolske, J. R.; Strahan, S. E.; Proffitt, M. H.; Webster, C. R.; May, R. D.; Fahey, D. W.; Baumgardner, D.; Dye, J. E.; Wilson, J. C.; Elkins, J. W.; Chan, K. R.; Anderson, J. G. *Science* **1993**, *261*, 1146.